# TIME LAPSE (4D) SEISMIC SIGNAL DETECTABILITY IMPROVEMENT USING CO-PROCESSING TECHNIQUE ON CARBONATE RESERVOIRS

**MOHAMED ABDELGHANY MOHAMED MAHGOUB**

**UNIVERSITI SAINS MALAYSIA**

**2023**

# TIME LAPSE (4D) SEISMIC SIGNAL DETECTABILITY IMPROVEMENT USING CO-PROCESSING TECHNIQUE ON CARBONATE RESERVOIRS

**by**

**MOHAMED ABDELGHANY MOHAMED MAHGOUB**

**Thesis submitted in fulfilment of the requirements for the degree of Doctor of Philosophy**

**November 2023**

## ACKNOWLEDGEMENT

I would like to thank the School of Physics at USM and Abu Dhabi National Oil Company (ADNOC) for encouraging and approving the use of ADNOC asset data for this research. I would like to thank Ms. Fatima Al Aryani, Geoscience Manager, for her great support in obtaining the approval of the confidentiality agreement between USM and ADNOC by the senior management of ADNOC. My sincere thanks also go to Mr. Yasir Almazrouei, ADNOC Upstream Executive Director, for his kind permission to use the asset data for this research. I am also very grateful to Mr. Mohamed Al Marzouqi, EVP of Development Function of ADNOC, for his support in granting permission to use the asset data for the research. I also thank CGG, the seismic service provider, for the use of Geovation seismic processing software to perform the seismic processing part of this study. I also thank Geosoftware for the use of Hampson Russell software to provide technical support for this research. I would like to thank my colleagues at ADNOC and the ADNOC Group for their help and support in conducting this research. I would like to thank my wife Nahed Sengar and my children Dr. Eman, Dr. Ahmed, Dr. Salma and my lovely youngest daughter Jannah for their constant encouragement in conducting my research. Finally, I would like to thank my main supervisor, Dr. Andy Anderson Bery, and my co-supervisors, Dr. Yasir Bashir (Faculty of Mines, Istanbul Technical University) and Dr. Abdelwahab Noufal (ADNOC), for the advice, guidance, and support they gave me throughout the research and publication. I am very grateful to my MSC supervisor, the great late Professor Dr. Deva Gosh of UTP, for inspiring me to do my PhD on 4D seismic in carbonate reservoirs.

## TABLE OF CONTENTS

**ACKNOWLEDGEMENT** ................................................ **ii**

**TABLE OF CONTENTS** ................................................ **iii**

**LIST OF TABLES** ................................................ **vi**

**LIST OF FIGURES** ................................................ **vii**

**LIST OF SYMBOLS** ................................................ **xx**

**LIST OF ABBREVIATIONS** ................................................ **xxii**

**ABSTRAK** ................................................ **xxiii**

**ABSTRACT** ................................................ **xxv**

**CHAPTER 1 INTRODUCTION** ................................................ **1**

1.1 Introduction ................................................ 1

1.2 Problem Statement ................................................ 4

1.3 Research Objectives ................................................ 5

1.4 Scope of Study ................................................ 6

1.4.1 Reservoir Background of the Study Area ................................................ 7

1.4.2 Phase 1 Summary ................................................ 10

1.4.3 Phase 2 Summary ................................................ 11

1.5 Novelty of the Research ................................................ 13

1.6 Layout of Thesis ................................................ 14

**CHAPTER 2 LITERATURE REVIEW** ................................................ **16**

2.1 Introduction ................................................ 16

2.2 4D Seismic Data Processing ................................................ 16

2.3 Pre-Stack Depth Migration ................................................ 18

2.4 Theory of Seismic Imaging by Least-Squares Inversion ................................................ 20

2.5 Time-Lapse (4D) Seismic in Carbonates ................................................ 28

2.6 Geography of the Study Area ................................................ 39

2.7 Study Area ........................................................................................ 40

2.8 Seismic Data Processing Vintages of the Research Field Cases .................... 42

2.9 Chapter Summary ................................................................................ 46

**CHAPTER 3 METHODOLOGY ............................................................... 48**

3.1 Introduction ........................................................................................ 48

3.2 Data Assembly ..................................................................................... 50

3.2.1 Seismic Data ..................................................................................... 51

3.2.2 Well Data .......................................................................................... 51

3.2.3 Supporting Documents ......................................................................... 51

3.3 Methodology ........................................................................................ 51

3.3.1 4D Seismic Co-Processing .................................................................... 55

3.3.2 4D Feasibility and Petroelastic Model ...................................................... 62

3.3.3 4D Seismic Joint Processing .................................................................. 65

3.4 Chapter Summary ................................................................................ 68

**CHAPTER 4 RESULTS AND DISCUSSION ................................................ 69**

4.1 Introduction ........................................................................................ 69

4.2 Research Results .................................................................................. 69

4.2.1 Results of 4D Feasibility Study ............................................................. 69

4.2.2 4D Pilot Studies Seismic Data Analysis ................................................... 77

4.2.3 Results of 4D Seismic Co-Processing ...................................................... 93

4.2.4 4D Seismic Attributes to QC the Co-Processing Results ............................ 106

4.2.5 Results of 4D Seismic Warping and Inversion ........................................... 116

4.2.6 Results of Supervising Machine Learning Approach .................................... 125

4.2.7 4D Seismic Signal Matching with Reservoir Performance ............................ 129

4.3 Utilization of 4D Seismic Co-Processing for the Research Cases .................. 148

4.4 Chapter Summary ................................................................................ 151

**CHAPTER 5 CONCLUSION AND FUTURE RECOMMENDATIONS ........ 152**

5.1 Conclusion ........................................................................................ 152

5.2 Limitations ....................................................................................... 153

5.3 Recommendations for Future Research ...................................................... 154

**REFERENCES .......................................................................................... 155**

**LIST OF PUBLICATIONS**

## LIST OF TABLES

**Page**

Table 2.1 4D Seismic Processing Routes. 17

Table 2.2 Math of LSM Seismic Processing Workflow after Perrone et al., 2018 24

Table 2.3 The Different Sensitivity of Predictability against NRMS after Detomo, 2013 38

Table 2.4 Case I, Seismic reprocessing and processing of the base and monitor. 43

Table 2.5 Case II, Seismic reprocessing and processing of base and monitor. 44

Table 2.6 Case III, Seismic reprocessing and processing of base and monitor. 45

Table 3.1 Seismic Acquisition Parameters of the 4D Surveys 49

Table 3.2 Reservoir Elastic Properties 65

Table 4.1 Scheme of Predictability Evaluation after Kragh and Christie (2002) 84

# LIST OF FIGURES

**Page**


| | | |
|---|---|---|
| Figure 1.1 | Case II; area of study: baseline 1994 3D OBC seismic acquisition (in yellow), and the new seismic acquisition 2013-2014 (red polygon). | 7 |
| Figure 1.2 | Case II; Phase 1 in red polygon and phase 2 in blue polygon outlines on the 1994 seismic acquisition survey (after Lafram et al., 2016). | 9 |
| Figure 1.3 | Case II; Monitor seismic acquisition survey (2013-2014) spread geometry layout. | 9 |
| Figure 1.4 | Case II; Phase 1 /Phase 2 comparison of the reservoir zonation (after Lafram et al., 2016). | 13 |
| Figure 2.1 | An iterative LSM algorithm workflow according to (Dong et al., 2017) | 21 |
| Figure 2.2 | (A) Seismic response of water replacing oil, (B) when gas replaces oil. (After Detomo, 2013). | 32 |
| Figure 2.3 | Velocity versus Effective Stress (After Detomo, 2013). | 33 |
| Figure 2.4 | Geographic locations of 4D seismic surveys in offshore Abu Dhabi, UAE (a) Case I, (b) Case II and (c) Case III. | 40 |
| Figure 2.5 | Jurassic and Cretaceous Stratigraphy of UAE, (Tamura et al., 2004). | 41 |
| Figure 3.1 | The flowchart of the research methodology shows the three phases of this study. | 54 |
| Figure 3.2 | Case I; seismic co-processing of baseline 2010 and monitor 2020. | 56 |
| Figure 3.3 | Case II; seismic co-processing of baseline 1994 and monitor 2014. | 58 |
| Figure 3.4 | Case III; seismic co-processing of baseline 2006 and monitor 2021. | 59 |

Figure 3.5 The 4D seismic least square migration (LSM) co-processing workflow. ......61

Figure 3.6 Proposed 4D Seismic Co-processing workflow for offshore seismic surveys. ......62

Figure 3.7 Physics model for carbonate rocks after Shiyu, Xu, and Michael Payne (2009) ......63

Figure 3.8 Fluid Substitution Saturated Properties after Gassmann (1951). ......64

Figure 3.9 Case I; vertical seismic section after the LSM: (a) monitor d1, before joint processing, (b) monitor Lm1 after joint processing, (c) monitor (d1-Lm1) is the difference section. (d) base survey. (lm2) before joint processing, (e) baseline Lm2 after joint processing, (f) base(d2-lm2) the difference section, (g) monitor Lm1 after joint processing, (h) base Lm2 after joint processing (i) lm2-lm1 the difference between base and monitor of joint processing. Yellow rectangular is enclosing the reservoir level difference......66

Figure 3.10 Case I; vertical seismic section after the LSM: Before joint processing; (a) base survey (b) monitor survey, (c) the difference section. After joint processing; (d) base survey. (e) monitor survey and (f) is the difference between base and monitor, yellow arrows are pointing out to reservoir level. ......68

Figure 4.1 Case II; (a) Gas production well; synthetic angle gathers for the in-situ and different water saturation scenarios,(b) the corresponding log tracks computed for the changes in VP, density and VS, for the in-situ and the different water saturation changes. ...70

Figure 4.2 Case II; (a) Gas production well: seismic synthetic angle stacks of differences between In-situ and 10% water saturation, (b) the difference between in-situ and 50% water saturation and (c) the difference between in-situ and 85% water saturation. ......71

Figure 4.3 Case II; (a) Water injection well; synthetic angle gathers for the in-situ and different water saturation scenarios, (b) the corresponding log tracks computed for the changes in VP, density and VS, for the in-situ and the different water saturation changes. ...72

Figure 4.4 Case II; (a) Water injection well: seismic synthetic angle stacks of differences between in-situ and 10% water saturation, (b) the difference between in-situ and 50% water saturation and (c) the difference between in-situ and 85% water saturation. .......................72

Figure 4.5 Case II; (a) Water injection well; synthetic angle gathers for the in-situ and different CO2 saturation scenarios, (b) the corresponding log tracks computed for the changes in VP, density and VS, for the in-situ and the different CO2 sweeping changes. .....73

Figure 4.6 Case II; (a) Water injection well: seismic synthetic angle stacks of differences between in-situ and 10% CO2 saturation, (b) the difference between in-situ and 50% CO2 saturation and (c) the difference between in-situ and 85% CO2 saturation..........................74

Figure 4.7 Case II; (a) cross-plot of P impedance (IP) versus IS (shear impedance) for three water saturation scenarios of the gas production well, (b) cross-plot of P impedance versus IS (shear impedance) for six water saturation scenarios of CO2 saturation of the water injection well, (c) ) cross-plot of P impedance versus VP /VS ratio for three water saturation scenarios of the gas production well, and (d) cross-plot of P impedance versus VP /VS for six water saturation and CO2 saturation scenarios of the water injection well. ............................................................................75

Figure 4.8 Case II; relative seismic inversion (full seismic bandwidth) of one subline seismic section: (a) base survey (b) monitor survey and (c) the difference between base and monitor. ....................................78

Figure 4.9 Case II; relative seismic inversion (30 Hz maximum frequency) of one subline seismic section: (a) base survey (b) monitor survey and (c) the difference between base and monitor...............................79

Figure 4.10 Case II; relative seismic inversion (15 Hz maximum frequency) of one subline seismic section: (a) base survey (b) monitor survey and (c) the difference between base and monitor...............................80

Figure 4.11 Case II; relative seismic inversion (full seismic bandwidth) of a time window between two horizons: (a) base survey (b) monitor survey and (c) the difference between base and monitor. Black arrows indicate higher impedance anomalies due to oil production and gas cap. ........................................................................... 81

Figure 4.12 Case II; relative seismic inversion (30 Hz maximum frequency) of a time window between two horizons: (a) base survey (b) monitor survey and (c) the difference between base and monitor. Black arrows indicate higher impedance anomalies due to oil production and gas cap. ..................................................................... 82

Figure 4.13 Case II; relative seismic inversion (15 Hz maximum frequency) of a time window between two horizons: (a) base survey (b) monitor survey and (c) the difference between base and monitor. Black arrows indicate high impedance anomalies due to oil production and gas cap. ..................................................................... 83

Figure 4.14 Case II; 3D seismic viewer of the pre stack migrated stack (a) base survey and (b) monitor survey. ................................................. 84

Figure 4.15 Case II; phase 2 pilot project, repeatability metric attribute for full seismic bandwidth time slice 1440 ms (a) Predictability of the base and monitor difference (b) Predictability histogram indicates moderate to good repeatability. ......................................................... 85

Figure 4.16 Case II; phase 2 pilot, Repeatability metric for full seismic bandwidth time slice 1440 ms (a) base, monitor, difference NRMS, (b) NRMS histogram showing NRMS 32% average value as pointed out by black arrow. ......................................................... 86

Figure 4.17 Case II; phase 2 pilot, time slice 1440 ms after high cut filter 30 Hz (a) base survey and (b) monitor survey. ....................................... 87

Figure 4.18 Case II; phase 2 pilot project, repeatability metric attribute for 30 Hz high-cut filter, time slice 1440 ms (a) Predictability of the base and monitor difference (b) Predictability histogram indicates good predictability higher than 85%. ................................................ 88

Figure 4.19 Case II; phase 2 pilot, Repeatability metric for 30 Hz high cut filter time slice 1440 ms (a) base, monitor, difference NRMS, (b) NRMS histogram showing NRMS 28% average value as pointed out by black arrow. 88

Figure 4.20 Case II; phase 2 pilot, time slice 1440 ms after high cut filter 15 Hz (a) base survey and (b) monitor survey. 89

Figure 4.21 Case II; phase 2 pilot project, repeatability metric attribute for 15 Hz high-cut filter, time slice 1440 ms (a) Predictability of the base and monitor difference (b) Predictability histogram indicates good predictability higher than 90%. 89

Figure 4.22 Case II; phase 2 pilot, Repeatability metric for 15 Hz high-cut filter time slice 1440 ms (a) base, monitor, difference NRMS, (b) NRMS histogram showing NRMS 24% average value as pointed out by black arrow. 90

Figure 4.23 Case II; phase 2 pilot, independent post stack time migration; one seismic subline section out of the base and monitor 3D volume (a) base survey, (b) the monitor survey and (c) the base, monitor difference section. Rectangular is highlighting zone of interest and arrows pointed out to coherent differences. 91

Figure 4.24 Case II; phase 2 pilot, jointly post stack time migration; one seismic subline section out of the base and monitor survey (a) base survey, (b) the monitor survey and (c) the base, monitor difference section. Rectangular is highlighting zone of interest and arrows pointed out to non-coherent differences. 92

Figure 4.25 Case II; phase 2 pilot, Predictability of base and monitor difference of time slice 1440 ms for the post-stack migrated (a) Independent post stack migration, (b) histogram showing lower predictability range, (c) Predictability of joint post stack migration and (d) histogram showing good repeatability higher than 85%. 92

Figure 4.26 Case I; offset and azimuth distribution difference between (a) monitor 2020 and (b) base (2010). 94

Figure 4.27 Case I; DSDR geometric of near COV of baseline survey; (a) classical binning showing less repeatability and (b) flexible binning which has less DSDR compared to the classical 4D binning and repeatability increased accordingly. .............................. 95

Figure 4.28 Case I; pre-stack depth seismic migrated stack with wells (vertical orange lines) of the 3D baseline survey (a) depth slice at 2855 m and (b) vertical seismic section with the reservoir level highlighted by the yellow arrow at 2.855 km depth. ......................... 96

Figure 4.29 Case I; depth slices of the reservoir level at 2855 m: (a) monitor KPSDM, (b) monitor LSM, (c) base KPSDM, and (d) base LSM. The crest of the structure is pointed out by a yellow arrow. .............. 97

Figure 4.30 Case I; vertical seismic section of 3D seismic volumes (a) base 2010 KPSDM, (b) monitor 2020 KPSDM, (c) the difference KPSDM between base and monitor, (d) base 2010 LSM, (e) monitor 2020 LSM, and (f) the difference of LSM between base and monitor. The reservoir level at 1.5 seconds is highlighted by yellow arrows, and the stack power of the reservoir level is greatly increased in the seismic LSM volumes. ................................ 98

Figure 4.31 Case I; comparison of seismic frequency octaves from the monitor survey: (a) KPSDM and (b) LSM. The yellow arrow points to the peak reservoir level. ..................................................... 99

Figure 4.32 Case II; horizon slice on a window between the upper and lower levels of the reservoir of the final migrated seismic stack volume (a) baseline seismic volume, (b) monitor seismic volume, and (c) the seismic difference between baseline and monitor surveys. The black polygon encloses the high amplitude difference at the crest of the reservoir structure. ................................................................ 100

Figure 4.33 Case III; vertical seismic section of KPSDM (a) base survey, (b) monitor survey, and (c) the 4D seismic difference between base and monitor. The yellow circle encloses a flat spot at the reservoir level. ........................................................................................ 101

Figure 4.34 Case III; vertical seismic section from LSM with final processing of (a) base survey, (b) monitor survey, and (c) the 4D seismic difference between base and monitor. The yellow circle encloses a flat spot at the reservoir level. ...................................................... 102

Figure 4.35 Case III; vertical seismic section of LSM with final processing including post-stack local matching of (a) baseline survey, (b) monitor survey and (c) the 4D seismic difference between base and monitor. The yellow circle encloses a flat spot at the reservoir level. ........................................................................................ 103

Figure 4.36 Case I; vertical seismic section of LSM volume (a) monitor with full seismic bandwidth, (b) base with full seismic bandwidth, (c) difference with full seismic bandwidth, (d) monitor30 Hz (e) base 30 Hz volume, and (f) the 30 Hz difference. The blue circle indicates the level of the reservoir. ................................................. 104

Figure 4.37 Spectral analysis of the signal-to-noise ratio on a subline of the 3D seismic volume (a) case I signal spectrum, (b) case I noise spectrum, (c) case II signal spectrum, and (d) case II noise spectrum. ........................................................................... 105

Figure 4.38 Autocorrelation window of an inline extracted over the 3D seismic volumes (a) Case I baseline survey and the black dashed line points to the terrain with periodic multiples, (b) Case I monitor survey, (c) Case II baseline survey, and (d) Case II monitor Survey. ................................................................... 106

Figure 4.39 Case I; 3D seismic attribute of the final migrated LSM stack; cosine of instantaneous phase at a time slice of 1500 ms (a) baseline image (b) monitor image. The white arrow points to the crest of the structure's reservoir. ..................................................... 107

Figure 4.40 Case I; 3D seismic coherency attribute of the cosine of the instantaneous phase volume at 1500 ms (a) baseline image and (b) monitor image. The blue arrow points to the crest of the structure. ........................................................................... 108

Figure 4.41 Case I; comparison of 4D metric NRMS attribute maps extracted at the 1500 ms reservoir level (a) KPSDM, (b) LSM. The ridge of the structure is indicated by a white arrow ...................................... 109

Figure 4.42 Case I; comparison of attribute maps of 4D metric predictability extracted at the 1500 ms reservoir level (a) KPSDM, (b) LSM. The black arrow points to the crest of the structure. ........................ 110

Figure 4.43 Case II; horizon slice of reservoir level (a) NRMS of KPSDM seismic volume, and (b) NRMS of LSM seismic volume. .............. 111

Figure 4.44 Case I; 4D cross plot between NRMS% and predictability % with histograms of NRMS and predictability in the upper and lower reservoir horizon window of the final migrated seismic volume of the KPSDM. ......................................................................... 112

Figure 4.45 Case I; 4D cross plot between NRMS% and predictability % with histograms of NRMS and predictability in the upper and lower reservoir horizon window of the final migrated seismic volume of the LSM. ............................................................................. 112

Figure 4.46 Case II; 4D cross-plot between NRMS% and predictability % with histograms of NRMS and predictability in the upper and lower reservoir horizon windows (a) KPSDM final migrated seismic volume and (b) LSM final migrated seismic volume.......... 113

Figure 4.47 Case III; 4D cross-plot between NRMS% and predictability % with histograms of NRMS and predictability in overburden horizon windows. ................................................................. 114

Figure 4.48 Case III; 4D cross-plot between NRMS% and predictability % with histograms of NRMS and predictability in the reservoir horizon windows. ................................................................. 115

Figure 4.49 Case III; 4D cross-plot between NRMS% and predictability % with histograms of NRMS and predictability, (a) unwarped seismic monitor and (b) warped seismic monitor. ........................... 116

Figure 4.50 Case III; vertical seismic section of 3D seismic volumes (a) LSM of 2010 base, (b) LSM of 2020 monitor, (c) the difference in

LSM between base and monitor, (d) LSM of 2010 base, (e) LSM of 2020 monitor after 4D time warping, and (f) the difference in LSM between base and warped monitor. The reservoir level between the upper and lower levels of the reservoir is highlighted by the black arrow, and the stack power of the reservoir level is greatly increased in the seismically warped LSM monitor volume. .......... 118

Figure 4.51 Case III; seismic difference time-slice at the reservoir level between (a) the baseline and un-warped seismic monitor survey and (b) the difference between the baseline and warped monitor. The black circle encloses the largest oil production cluster. .......... 119

Figure 4.52 Case I; a time window around the reservoir horizon with black polygon around the amplitude anomaly (a) 4D warping; time shift DT and (b) velocity variation DV. The black arrow points to the negative DT and the positive DV inside the block polygon. .......... 120

Figure 4.53 Case II; (a) time shifts DT and (b) velocity change DV. The black circle encloses the apex of the reservoir. The black arrow indicates the downward time shift and decreasing velocity. .......... 121

Figure 4.54 Case III; (a) time shifts DT and (b) velocity change DV. The white circle encloses the large cluster of oil production. The black arrow indicates upward time shifts and increasing velocity. .......... 122

Figure 4.55 Case I; a time window horizon slice of the RMS amplitude with a black polygon around the amplitude anomaly (a) overburden zone (b) reservoir zone and (c) the under burden zone. .......... 123

Figure 4.56 Case III; a time window horizon slice of the RMS amplitude with a polygon around the amplitude anomaly (a) overburden zone (b) reservoir zone and (c) the underburden zone. Black arrows point out to the production clusters A and B. .......... 124

Figure 4.57 Case I; a time-window horizon slice of the 4D inversion P-impedance difference with a polygon around the amplitude anomaly (a) overburden zone, (b) reservoir zone, and (c) the underburden zone. Black arrows indicate the locations of high impedance. ....................................................................... 125

Figure 4.58 Case II; predicted density from well logs and seismic inverted volumes overlying well logs with original density, (a) 13 well log traces, (b) six well log traces, (c) DFNN six well log tracks, (d) 13 wells, that match between predicted and actual density, (e) 6 well logs that match between predicted and actual density, and (f) 6 well logs that match between predicted and actual density using machine learning with DFNN. The blue rectangle encloses the interval of reservoir logging. The target logs are coloured black, while the predicted logs are red. The blue arrow indicates the similarity of the actual and predicted densities of six well logs with and without machine learning with DFNN, and the black oval highlights the fit. ....................................................... 127

Figure 4.59 Case II; a subline over the predicted seismic density volume with the actual density log of the intersected well (a) 13 wells used to train and validate the data, (b) 6 wells used to train and validate the data, and (c) 6 wells with the machine learning approach. The black rectangle encloses the reservoir interval, and the black arrow indicates the resolution differences between the different paths. ............................................................................. 128

Figure 4.60 Case II; reservoir horizon slice (a) DV velocity variation between baseline and monitor survey, (b) P impedance of seismic monitor survey, (c) monitor-predicted density, and (d) monitor-predicted porosity. The decrease in DV, impedance, and density and the increase in porosity are indicated by the black arrow. .................... 129

Figure 4.61 Case I; reservoir production over the year (a) water cut % and GOR (SCF /STP, Standard Cubic feet per Standard Temperature and Pressure) and (b) average pressure changes in the reservoir over time.......................................................................... 130

Figure 4.62 Case I; (a) Cumulative water cut percentage over time and (b) Sum of cumulative water production volume in BBL over time. .... 131

Figure 4.63 Case I; relationship between 4D seismic signal anomaly polygon and oil sector distribution (a) 4D seismic anomaly polygon with inverted acoustic impedance (b) contour map of reservoir closure contour with well sector 4 polygon above. .....................................132

Figure 4.64 Case I; the relationship between the 4D seismic signal and the production data shows the pressure changes: (a) average pressure in 2010 and (b) average pressure in 2020. ......................................133

Figure 4.65 Case I; The relationship between the 4D seismic signal and production data shows the fraction of water saturation per pore volume: (a) the average water saturation in 2010 and (b) the average water saturation in 2020, blue arrows indicate higher sweeping water spots throughout the field......................................134

Figure 4.66 Case I; the relationship between the 4D seismic signal and production data shows the fraction of oil saturation per pore volume: (a) average oil saturation in 2010 and (b) average oil saturation in 2020. The black arrow indicates oil saturation decreasing spot throughout the field. ..............................................135

Figure 4.67 Case I; the relationship between reservoir water saturation and the percentage of impedance change between baseline and monitor surveys, (a) average water saturation in 2020, and (b) horizon slice of the difference between baseline and monitor impedance % at the reservoir level. The blue arrows indicate larger water spots throughout the field and high impedance changes on the horizon slice. ..........................................................136

Figure 4.68 Case II; reservoir performance over time (a) water injection, (b) gas injection. The white arrow shows the changes in water and gas injection between the 1994 base year and the 2014 year of the monitor survey. ...................................................................................137

Figure 4.69 Case II; reservoir performance over time (a) oil, gas, and water saturation in Mscf/day and (b) water cut %. White arrow indicates the variations in oil, water, and gas saturation and water cut variations in 1994 and 2014 (seismic time lapse). .....................138

Figure 4.70 Case II; cross-plot of Porosity versus Permeability in unit total with average pressure as colour code of the reservoir crest zone. ... 139

Figure 4.71 Case II; reservoir performance over time-average pressure changes (a) 1994 baseline (b) 2014 monitor and (c) difference in pressure between baseline and monitor. The apex of the structure is indicated by a red polygon and a black arrow indicating the maximum pressure difference. ... 139

Figure 4.72 Case II; reservoir performance over time of average saturation (a) oil saturation baseline 1994 (b) oil saturation monitor 2014, (c) oil saturation difference, (d) water saturation baseline 1994, (e) water saturation monitor 2014, and (f) water saturation difference. The black arrow on the polygon indicates the significant decrease and increase in oil and water saturation, respectively. ... 140

Figure 4.73 Case II; (a) Changes in pressure saturation over the 20-year period and (b) horizon slice difference between baseline and monitor survey. The black polygon shows the average pressure difference and the higher amplitude of the seismic difference. ... 141

Figure 4.74 Case III; reservoir performance over time. The black arrow indicates the changes in oil and water saturation, increasing from 2006 to 2020; the blue circle encloses the mixing of water and oil production in 2008. ... 142

Figure 4.75 Case III; (a) water saturation in 2006, and (b) water saturation in 2020. The black circle encloses the area with well production clusters. ... 143

Figure 4.76 Case III; (a) reservoir pressure in 2006 and (b) reservoir pressure in 2020. The black circle encloses the area of the wells production clusters. ... 144

Figure 4.77 Case III; reservoir horizon (a) seismic amplitude difference and (b) P-impedance difference. The white polygon encloses the area of the major oil production zone, and the black arrow indicates time-lapse changes in the reservoir. ... 145

Figure 4.78 Case III; Acoustic hardening, white polygon is enclosing the area of the big production zone with black arrow points to the changes in the reservoir over the time-lapse. ................................................ 146

Figure 4.79 Case III; predicted water saturation at the reservoir level (a) the baseline survey (b) the monitor survey and (c) the difference water saturation. ................................................................... 146

Figure 4.80 Case III; (a) map of saturation difference between base and monitor and (b) NRMS at the reservoir level. ................................. 147

Figure 4.81 Case III; (a) map of saturation difference between base and monitor, and (b) RMS at the reservoir level. ................................... 148

## LIST OF SYMBOLS

| | |
|---|---|
| d | The seismic data |
| L | The Kirchhoff forward modelling operator |
| r | Subsurface reflectivity |
| m | The Kirchhoff migration |
| $L^H$ | The adjoint of the Kirchhoff forward operator |
| $r_{LS}$ | The subsurface reflectivity |
| $L^H$L | Hessian operator |
| f(r) | The cost function of least-square migration |
| Q | Seismic waves absorption compensation quality factor |
| $LQ$ | Kirchhoff visco-acoustic modelling operator |
| $(\mathrm{L}^{\mathrm{H}}\mathrm{L})^{-1}$ | Hessian operator inverse |
| RMS | Root mean Square. |
| NRMS | Normalized Root Mean Square. |
| $\mathrm{a_i}$ | Base survey trace. |
| $\mathrm{b_i}$ | Monitor survey trace. |
| $\mathrm{t1} - \mathrm{t2}$ | A given time window |
| $\mathrm{C_{bm}}$ | Cross-correlation of baseline and monitor trace within a given time window. |
| $\mathrm{C_{bb}}$ | Auto-correlation of baseline trace. |
| $\mathrm{C_{mm}}$ | Auto-correlation of monitor trace. |
| τ | Tau which equals to 300. |
| π | Pi is the ratio of the circumference of any circle to the diameter of that circle. In decimal form, the value of pi is around 3.14. |
| $LM$ | The linear modelling operator L, M is the reflectivity model. |
| $d$ | The seismic data. |
| $d_0$ | The baseline survey |
| $d_1$ | The monitor survey. |
| $m_0$ and $m_1$ | The baseline and monitor reflectivity models. |
| $L_0$ and $L_1$ | The baseline and monitor modelling operators. |
| $S$ | Quadratic Cost function |
| $\widetilde{m_0}$ and $\widetilde{m_1}$ | Migrated images of baseline and monitor |
| $\acute{L_0}$ and $\acute{L_1}$ | Base and monitor migration operators. |
| $L_0$ and $L_1$ | Base and monitor modelling operators. |
| $H_0$ and $H_1$ | The Hessian matrices. |
| $\Delta\widehat{m}$, | Inverted time-lapse image. |

| | |
|---|---|
| $dV$ | The velocity variation. |
| $\Delta t/t$ | Time variation and two-way travel time. |
| $\Delta z/z$ | The variation in thickness and the thickness. |
| $Szz$ | The total vertical stress variation. |
| $Sxx$ | Stress in the x-direction. |
| $Syy$ | Stress in the y-direction. |
| Ezz | The vertical strain. |
| $R$ | The dimensionless parameter. |

## LIST OF ABBREVIATIONS

| | |
|---|---|
| 4D | The time-lapse $4^{th}$ dimension |
| 5D | Five dimensions; inline/crossline/offset/ azimuth, and time dimension |
| Co-processing | Same processing sequence applied on base and monitor seismic surveys |
| COV | Common Offset Vector |
| DSDR | Source & Receiver distance |
| Hz/DB | Hertz, measuring frequency unit for. Decibel, amplitude measuring unit |
| IP | Impedance of P (Compressional seismic waves) |
| IS | Impedance of S (Shear seismic waves) |
| KPSDM | Kirchhoff Pre-Stack Depth Migration |
| LSM | Least Square Migration |
| LSRTM | Least Square Reverse Time Migration |
| OBC | Ocean Bottom Cable |
| OBN | Ocean Bottom Node |
| OVTs | Offset Vector Tiles |
| PETREL | Seismic interpretation software |
| PreSDM | Pre-Stack Depth Migration |
| PreSTM | Pre-Stack Time Migration |
| PU | Per Unit |
| PZ | P (hydrophone receiver which is pressure gradient) and while the collocated geophone is recording Z, the vector displacement of the seabed. |
| RMO | Residual Moveout |
| RMS/NRMS | Root Mean Square/Normalized Root Mean Square |
| RTM | Reverse Time Migration |
| SW | Saturation Water |
| TL | Time Lapse |
| TWT | Two Way Time |
| USM | Universiti Sains Malaysia |
| DAS | Distributed Acoustic Sensing |
| VSP | Vertical Seismic Profile |

**PENINGKATAN PENGESANAN ISYARAT SEISMIC SELANG MASA (4D) MENGGUNAKAN TEKNIK PEMPROSESAN BERSAMA BAGI TAKUNGAN KARBONAT**

## ABSTRAK

Kajian seismik 4D digunakan untuk memantau prestasi takungan hidrokarbon semasa fasa pengeluaran atau suntikan. Tinjauan seismik 3D yang berulang mesti dapat mengukur isyarat 4D yang dapat mengesan penggantian cecair atau perubahan tekanan yang mungkin berlaku semasa pengeluaran takungan atau suntikan air atau gas dalam sesuatu tempoh masa. Secara praktiknya, isyarat seismik yang digabungkan dengan perubahan sedemikian boleh dilihat dalam takungan klastik sedangkan ia boleh diabaikan dalam takungan karbonat yang berheterogeni. Mengulangi kaji selidik seismik 3D dengan geometri pemerolehan yang sama biasanya sukar di Timur Tengah kerana perubahan alam sekitar (contohnya, rupa bumi kasar, arus air, perubahan bermusim, dan pemasangan pengeluaran lapangan). Oleh itu, tiga medan minyak dan gas di luar pesisir Abu Dhabi di Emiriah Arab Bersatu dengan kebolehulangan pemerolehan seismik yang terhad telah dipilih untuk kajian ini. Dalam kajian ini, pemprosesan bersama seismik 4D untuk tiga kajian kes berbeza daripada input data, sama ada ia bermula dari data medan seismik atau dari pra-pemprosesan dan penyahkonvolusi yang berbeza, atau sama ada ia bermula selepas deconvolusi yang sama pada asas dan memantau survei seismik. Penyelidikan seismik 4D ini bermula dengan kajian kebolehlaksanaan 4D berasaskan kajian 1D untuk menentukan kebarangkalian isyarat 4D dari data log di telaga minyak semasa melakukan pemprosesan bersama seismik 4D tinjauan asas dan pemantauan. Pelengkungan dinamik pengesan 4D dikira untuk tinjauan survei,

menggunakan tinjauan asas sebagai rujukan untuk mendapatkan penyongsangan 4D seismik penentu yang tepat. Penggabungan balak yang baik dan jumlah seismik telah diuji untuk meramalkan jumlah sifat log di lokasi telaga jumlah penyongsangan seismik. Pembelajaran mesin yang diselia, Deep Feed Forward Neural Network (DFFNN), juga diuji menggunakan log yang relevan dari enam telaga untuk melatih dan mengesahkan data. Jumlah ketumpatan dan keliangan seismik 3D dicipta untuk tinjauan asas dan pemantauan dan dipadankan dengan ketumpatan dan keliangan balak dari telaga. Penyelidikan inovatif ini telah menggunakan langkah yang tepat untuk membuat pemprosesan bersama dengan seismik 4D untuk menunjukkan kebolehulangan seismik yang rendah. Ia juga telah membuktikan bahawa ketepuan yang kuat dan perubahan tekanan dalam takungan dapat mengesan isyarat seismik 4D lebih baik daripada memastikan kebolehulangan pemerolehan seismik yang sempurna. Bagi tiga lokasi di luar pesisir yang digunakan dalam kajian ini, penyelidikan ini dapat membantu mengoptimumkan penempatan telaga minyak yang lebih yang tepat untuk mencapai kawasan takungan yang baik dan tidak terganggu supaya telaga minyak dapat memberikan penghasilan maksimum dengan menangguhkan air dan gas daripada pengeluaran.

**TIME LAPSE (4D) SEISMIC SIGNAL DETECTABILITY IMPROVEMENT USING CO-PROCESSING TECHNIQUE ON CARBONATE RESERVOIRS**

## ABSTRACT

4D seismic studies are used to monitor the performance of hydrocarbon reservoirs during production or injection phases. Repeated 3D seismic surveys must be able to measure a 4D signal that can detect fluids substitution or pressure changes that may take place during reservoir production or injection of water or gas over a period of time. In practice, the seismic signal allied with such changes could be perceptible in clastic reservoirs whereas it could be negligible in heterogeneous carbonate reservoirs. Repeating 3D seismic surveys with the same acquisition geometry is usually difficult in the Middle East due to environmental changes (e.g., rough terrain, water currents, seasonal changes, and field production installations). Therefore, three oil and gas fields of offshore Abu Dhabi in the United Arab Emirates with scarce seismic acquisition repeatability have been selected for this study. In this study, the 4D seismic co-processing for the three case studies differs from the input data, whether it starts from the seismic field data or from different pre-processing and deconvolution, or whether it starts after the same deconvolution on base and monitor seismic surveys. This 4D seismic research began with a 1D well-based 4D feasibility study to determine the probability of 4D signals from the borehole logs while performing 4D seismic co-processing of the baseline and monitoring surveys. A 4D trace dynamic warping was computed for the monitor survey, using the baseline survey as a reference to obtain an accurate deterministic seismic 4D inversion. Merging well logs and seismic volumes was tested to predicting a volume of log properties at the well locations of the seismic inversion

volume. Supervised machine learning, Deep Feed Forward Neural Network (DFFNN), was also tested using relevant logs from six wells to train and validate the data. 3D seismic volumes of density and porosity were created for the baseline and monitoring surveys and matched to the density and porosity logs from the wells. This innovative research has developed best practices for 4D seismic co-processing for such low seismic repeatability. It has also proven that strong saturation and pressure changes in reservoirs can detect the 4D seismic signal better than ensuring perfect seismic acquisition repeatability. For the three offshore fields used in this study, this research could help optimize the proper placement of infill wells to reach the undrained areas of the reservoirs so that the wells can provide maximum recovery with delayed water and gas breakthrough.

# CHAPTER 1

# INTRODUCTION

## 1.1 Introduction

While the extraction of hydrocarbons from carbonates represents a significant portion of the world's energy resource, 4D seismic is more widespread and successful in clastic reservoirs than in carbonate reservoirs (Sarkar et al., 2003; Calvert, 2005). The heterogeneity of carbonate rocks and difficult rock physics challenges, such as the high stiffness of the rock frame, could complicate the use of 4D seismic to monitor fluid changes in carbonate rocks. The seismic industry still believes that seismic acquisition repeatability is the most important success factor for meaningful 4D seismic analysis for both clastic and carbonate reservoirs. Despite the high cost of acquisition, time-lapse processing is an indispensable factor to obtain highly repeatable data (Smith et al., 2019).

Repeatability of seismic acquisition in the development areas cannot be readily guaranteed because there are more rigs, wellhead production platforms, pipelines, and infrastructure that could make it impossible to place the sources and receivers in the same location after the production period is over. In the study areas, 4D seismic surveys were conducted with different geometries of the baseline and monitor, and the 4D seismic analysis went beyond the usual way of focusing only on the seismic amplitude difference between the baseline and monitor. The creation of a petroelastic model and a 1D wellbore-based 4D feasibility study was an exceptional step in predicting the 4D signal from the wellbore information. Simulation of different water and gas injection scenarios shows the effects on impedance of compressional and shear waves and VP / VS changes. In addition, these changes were matched with changes in fluid and gas saturation in the reservoir over time.

One of the main objectives of this research was to develop an ideal workflow for 4D seismic that can bridge the poor repeatability of seismic acquisition. In this study, joint base and monitor 4D seismic processing was tested using Kirchhoff Pre-Stack Depth Migration (KPSDM), the common seismic best practice, against Kirchhoff Pre-Stack Depth Migration Least Square Migration (LSM). LSM was found to have a lower average Normalized Root Mean Square (NRMS) value compared to KPSDM. Typical NRMS values for offshore fields in the literature range from 10% to 25% (Detomo, 2013).

For optimal calculation of dynamic time and space warping, multiple monitor surveys must be matched with a baseline survey (Hampson et al., 2005). The accuracy of dynamic time warping (DTW) in similarity estimation is being investigated for template matching and clustering of seismic traces (Kumar et al., 2022). In addition, the alignment of baseline and monitor seismic volumes in the time and depth domains has resulted in amplitude and time convergence of these two volumes. Time shifts and amplitude variations between the baseline and monitor surveys were also investigated to track fluid exchange and pressure changes. 3D seismic volumes with velocity variations were also created by scripting the 3D time-shift volumes to create the low-frequency model of the monitor, which was combined with the low-frequency baseline model to obtain the 4D seismic inversion result.

Choosing a robust analysis domain is particularly important in 4D time-lapse studies (Rafael et al., 2017), so 4D seismic inversion can be more effective than systematic seismic wiggle-trace work in this regard. (Tarantola, 2005) has described seismic inversion as the conversion of seismic reflections into elastic physical properties of the subsurface. Such elastic properties may be related to porosity, lithology, fluid saturation, and geomechanical properties (Frazer et al., 2008). The goal of time-lapse seismic inversion is to predict changes in elastic rock properties, such as acoustic impedance (Daiane et al., 2020). In addition, the goal is to define a reservoir model that has less error between predicted and observed seismic amplitudes (Francis, 2005).

It is a fact that the reflectivity of water-bearing reservoirs increases with water saturation and decreases with decreasing frequency. The fluid in the reservoir induces a low-frequency anomaly in the seismic spectral decomposition, while a high-frequency anomaly is induced by the gas or clay content in the reservoir (Goloshubin et al., 2005). Spectral decomposition was also extracted in the third case of this study to relate frequency changes to changes in fluid and gas saturation in the seismic time course of the baseline and monitor record. Vertical 4D resolution (ideally 1-10 m) is the main challenge in 4D seismic. For carbonate reservoirs, seismic repeatability could be improved by using innovative methods to acquire 4D seismic with reservoir measurements and simulation techniques (Amundsen and Landrø, 2007). In this study, a hybrid theory and data model was used to evaluate 4D seismic inversion results and predict changes in reservoir rock properties, such as density and porosity, over the period of production from baseline and monitor surveys.

To establish a link between the logs and the seismic data at the well sites, Hampson Russell (Emerge) software was used. In geophysics, neural network is used to quantitatively predict rock properties from seismic data (Downton, 2018). In supervised machine learning, the neural network uses a set of inputs and outputs for a given trick and the relationship between inputs and outputs is determined. The disadvantage of this deep learning approach is that there must be enough inputs and outputs to adequately train the network (Hampson et al., 2001).

For Case II, 3D seismic volumes for density and porosity were created. They can be used to determine the best places to fill wells when there are areas of low density and high porosity in the reservoir that are undrained. Porosity and permeability changes in time-lapse production were matched with pressure changes in the reservoir that could explain reactivation of faults in the monitor survey. The changes in reservoir performance were matched with the observed 4D signal in seismic time-lapse for the three case studies in this research. The mechanism of 4D signal generation was investigated using the changes in water and oil saturation and pressure.

## 1.2 Problem Statement

Seismic acquisition repeatability is a challenge when it comes to maintaining the same shot and receiver position throughout the production period. Enhanced oil recovery (EOR) or CO2 removal will encounter some difficulties in carbonate reservoirs, which generally have difficult reservoir characterization. The oil and gas industry also still relies on standard seismic imaging algorithms such as pre-stack Kirchhoff time and depth imaging. Both are not forgiving of geometric irregularities and poor repeatability of seismic imaging. Moreover, residual differences in time, phase, amplitude, frequencies, and background noise after cross equalization are the major obstacles to all 4D seismic monitoring surveys. The weak 4D signal is unable to detect changes in the reservoir due to production or injection activities. Seismic interpretation of 4D seismic in carbonate is not common to date because there are no relevant seismic attributes to help with quantitative interpretation of 4D seismic.

Various studies on 4D seismic consider that 4D in carbonate reservoirs is still a major challenge and is still in the pilot and test phase and is very rarely used at production scale. In addition, the repeatability of seismic images is not optimally guaranteed. 4D is not credible enough to be used for reservoir monitoring. (Lafram et al., 2016) has shown that the 4D signal can interpret water intrusion, gas re-dissolution, and gas cap extension on 4D with the same acquisition repeatability. However, with different acquisition geometries, it was found that the gas cap expansion could not be interpreted, but the water motion could. To date, no complete 4D seismic analysis has been published, demonstrating that 4D is a model for integration: acquisition of 4D feasibility, propagation through 4D seismic co-processing to dynamic 4D trace warping cascaded through 4D seismic inversion, and finally reconciliation of results with reservoir saturation and pressure changes throughout the 3D seismic period.

## 1.3 Research Objectives

The main purpose of time-lapse (4D) seismic surveys is to monitor reservoir surveillance and optimize well plugging in a production field. It is also to monitor fluid and gas injection in the reservoir to improve the EOR or IOR. To achieve the goals, we have the following objectives:

i. To determine whether 4D seismic acquisition in carbonate reservoirs can be generally successful and when the repeatability of seismic acquisition is low in particular. Acquiring repeated surface seismic baseline and monitor surveys in development fields cannot be perfectly guaranteed.

ii. To develop the best 4D seismic co-processing sequence that could close the gap of low repeatability of seismic acquisition, and to verify whether seismic imaging such as LSM alone can improve the repeatability of seismic acquisition. Nevertheless, seismic co-processing, starting from pre-processing, such as noise reduction, deconvolution, passing through demultiple to LSM pre-stack depth migration, is the best sequence to increase repeatability by joint seismic processing.

iii. Integrate 4D seismic co-processing results with production and injection data to match 4D seismic signatures with reservoir fluid substitution and pressure changes over seismic time-lapse and understand the mechanism of 4D generation.

## 1.4 Scope of Study

To evaluate the feasibility of a meaningful 4D seismic study in carbonate, the reservoir background of the three cases in this study was investigated. The results of the 4D pilots from Case II, one of the giant offshore fields in Abu Dhabi, UAE, were the motivation for conducting this study. The analysis of the results of these 4D pilots is detailed later in this study.

### 1.4.1 Reservoir Background of the Study Area

In the case II, 3D OBC seismic survey was conducted over this producing field in December 2013 and completed in November 2014 (Figure 1.1). It was decided to take the opportunity of the current seismic acquisition to conduct a pilot 4D survey over 24 km² of the area of interest (Phase-1). Three swaths were acquired as monitors, using the same seismic acquisition geometry (base) from 1994 for this 4D study.

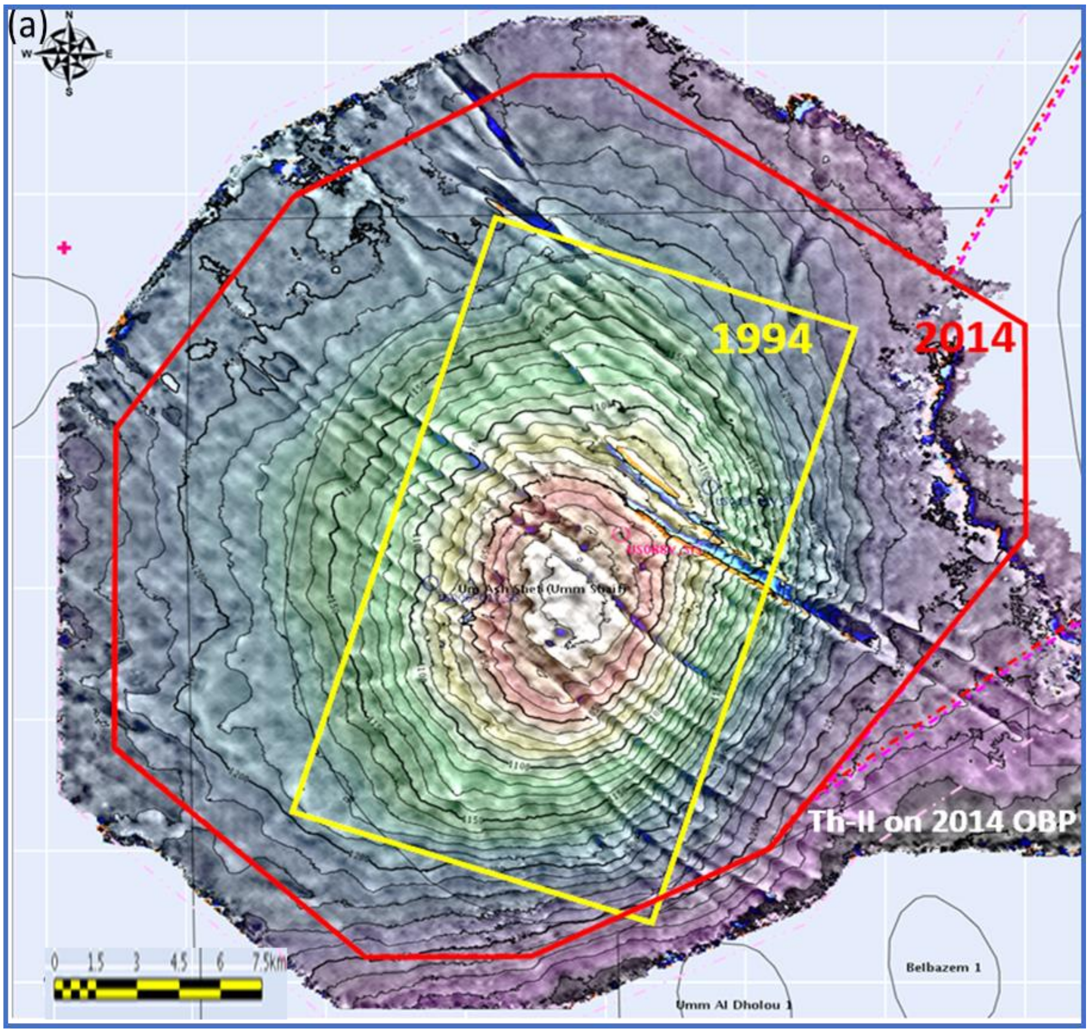


Figure 1.1 Case II; area of study: baseline 1994 3D OBC seismic acquisition (in yellow), and the new seismic acquisition 2013-2014 (red polygon).

This acquisition was an exclusive opportunity to determine the 4D signal in this offshore carbonate environment in the target reservoir of Abu Dhabi, UAE (Lafram et al., 2016). The objective of this Phase 1 4D pilot study was to test whether a reliable 4D signal could be identified above the noise level. This Phase 1 pilot study, using the same repeated geometry of base and monitor, successfully demonstrated that a 4D signal is measurable at the reservoir level of this field after a seismic time-lapse of 20 years of production.

A more sophisticated phase 2 was then initiated, using the new, completely different acquisition design as a monitor over a 57 $km^2$ test area. The second phase is a cross-sectional acquisition with a wide azimuth so that the baseline acquisition with a narrow azimuth is not repeated (Figure 1.2). More specifically, shots direction was almost 70° to the Phase 1 shot direction, which is very unfavourable in terms of repeatability. In addition, different sources and sensors were used (an array of 4 velocity meter in the baseline seismic and single accelerometers for the monitor seismic). The layout of the acquisition geometry of the new seismic acquisition consists of orthogonal overlapping zippers with 8 receiver lines and 4 receiver line rolls (Figure 1.3).

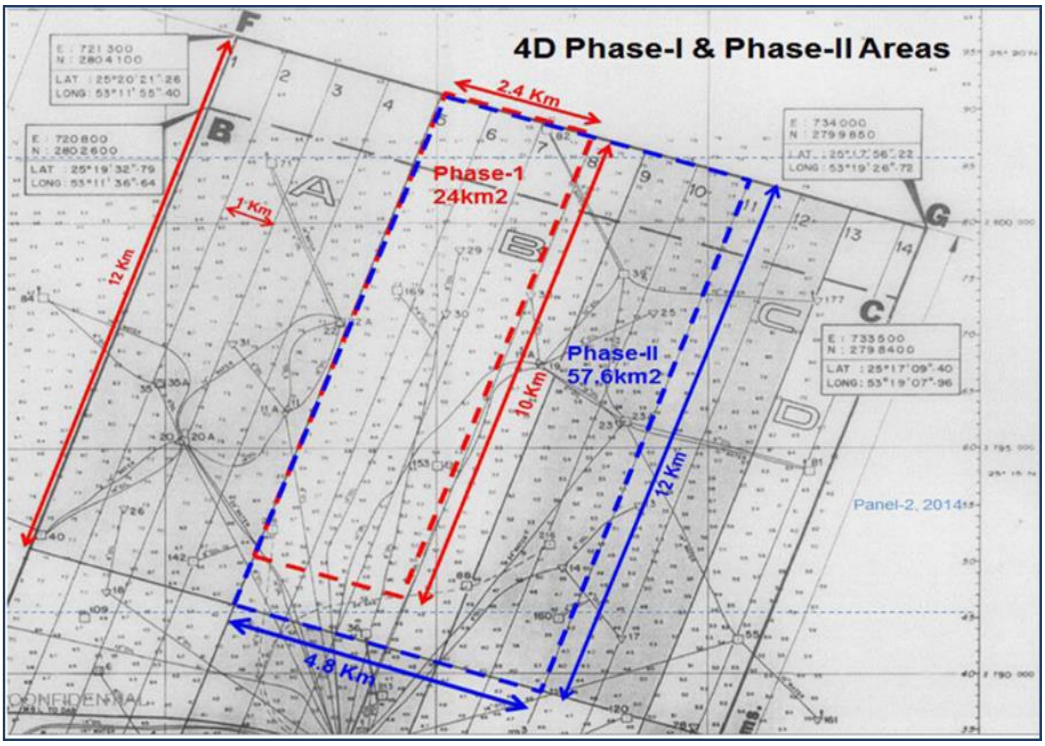


Figure 1.2 Case II; Phase 1 in red polygon and phase 2 in blue polygon outlines on the 1994 seismic acquisition survey (after Lafram et al., 2016).

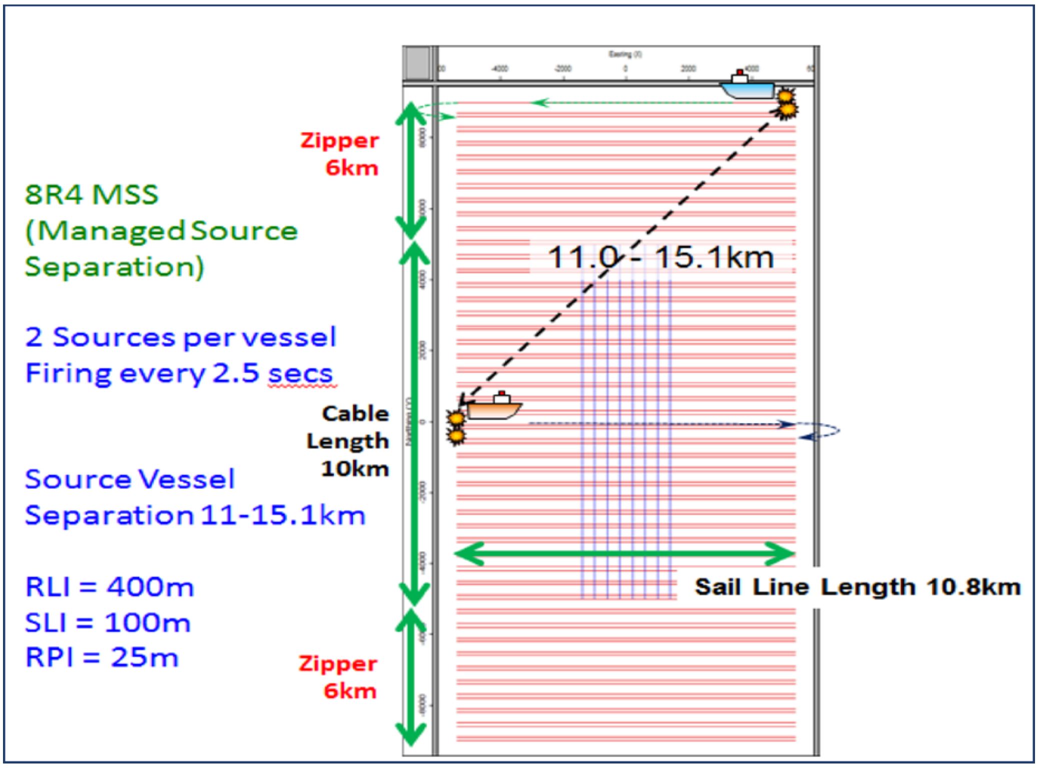


Figure 1.3 Case II; Monitor seismic acquisition survey (2013-2014) spread geometry layout.

The experience gained in Phase 1 also provided a good understanding of the global processing challenges. The interpretation results validated the processing sequence used at that time. Phase 2 needed to address the new challenges described above, and so a processing strategy was developed and updated throughout the project. The first challenge was to find the optimal denoising and de-multiple strategy with the most appropriate data modelling and subtraction in both surveys. In addition, 4D binning with the selection of the most repeatable traces without decimating too many traces was also a challenge. The second major challenge was to mitigate acquisition-related time and amplitude biases, combat the remaining non-repeatable multiples and non-repeatable coherent noise, optimizes muting, and carefully fit very different data.

It has proven to be very beneficial to have a systematic and consistent QC strategy for these very demanding pilots. Much research was conducted before the optimal workflow was developed. For some key steps, it was imperative to advance QC to seismic inversion/warping. As expected, analysis of the final products from Phase 2 shows higher repeatability noise compared to Phase 1, but initial QC after processing has yielded useful information.

### 1.4.2 Phase 1 Summary

In the Phase 1 summary, the 4D signal was found to be coherent in the reservoir:

- Coherent with the structural scheme (Figure 1.4)
- Coherent with the dynamic data from the wells (gas/water production)
- Coherent with the phenomena expected from the reservoir model.

One of the most important points is that the water rise can be detected, and the upper water surface can be determined at the time of monitoring. The role of the barrier at a certain level in the reservoir is well seen in the 4D data. Other production phenomena (expected from the dynamic model) such as pressure decay, gas rebound, and gas cap expansion can be interpreted in 4D. This experiment demonstrates that 4D seismic imaging in carbonates offshore Abu Dhabi (United Arab Emirates) is feasible under certain conditions for repeatability of data acquisition and with careful planning and execution of processing in a challenging seismic environment. Quality control and correction of data integrity, extensive denoising sequencing, demultiple, and correction of acquisition-related biases was necessary to reveal the 4D signal.

### 1.4.3 Phase 2 Summary

Several details identified during the interpretation of Phase 1, such as the extent of the gas cap in small heterogeneities and localized areas of overpressure. Those areas are difficult to find in Phase 2 (Figure 1.4); however, the 4D signal associated with water movement is robust and can be interpreted. This 4D signal was calibrated with production wells and the key issues in interpreting the 4D signal associated with water movement are as follows:

i. The boundaries of areas crossed by water can be mapped separately.

ii. Water is visible and can be mapped with 4D seismic in the eastern part of the phase 2 area.

iii. Moreover, 4D shows that water has advanced further south in 2014.

iv. The 4D interpretation shows that the water can follow a non-matrix path in some areas and finds a preferred path through fractures and structural lineaments.

The full study of the pilot phase, phase I, and phase II clearly shows that the most important parameter limiting repeatability is the ability to place the sensors and shots well, as was the case in the baseline study. This is critical for two reasons: avoidance of wave propagation bias due to local, surface changes in the subsurface and the ability to select the same subset of data for multiple processing steps. In addition, the random noise was very high in the OBC acquisition for both phases (ADNOC internal reports not published).

In Phase 1 of the pilot with the same baseline and monitor acquisition geometry, the NRMS is 13%, while in Phase 2 with a different baseline and monitor acquisition geometry, it is 28%. Seafloor currents, Schulte surface waves, and ship noise are hard on OBC seismic cables laid on the seafloor. While the Ocean Bottom Node (OBN) wirelesses system is highly recommended for seismic acquisition, especially because of the shallow water in this offshore field in Abu Dhabi, UAE. ADNOC has conducted the world's largest 3D onshore and offshore seismic surveys in Abu Dhabi using very high seismic acquisition parameters specifications. For offshore seismic, a 3D OBN seismic acquisition type was selected to provide seismic fold coverage of 2400 with 6 km of inline and crossline offsets, (Cambois et al., 2019).

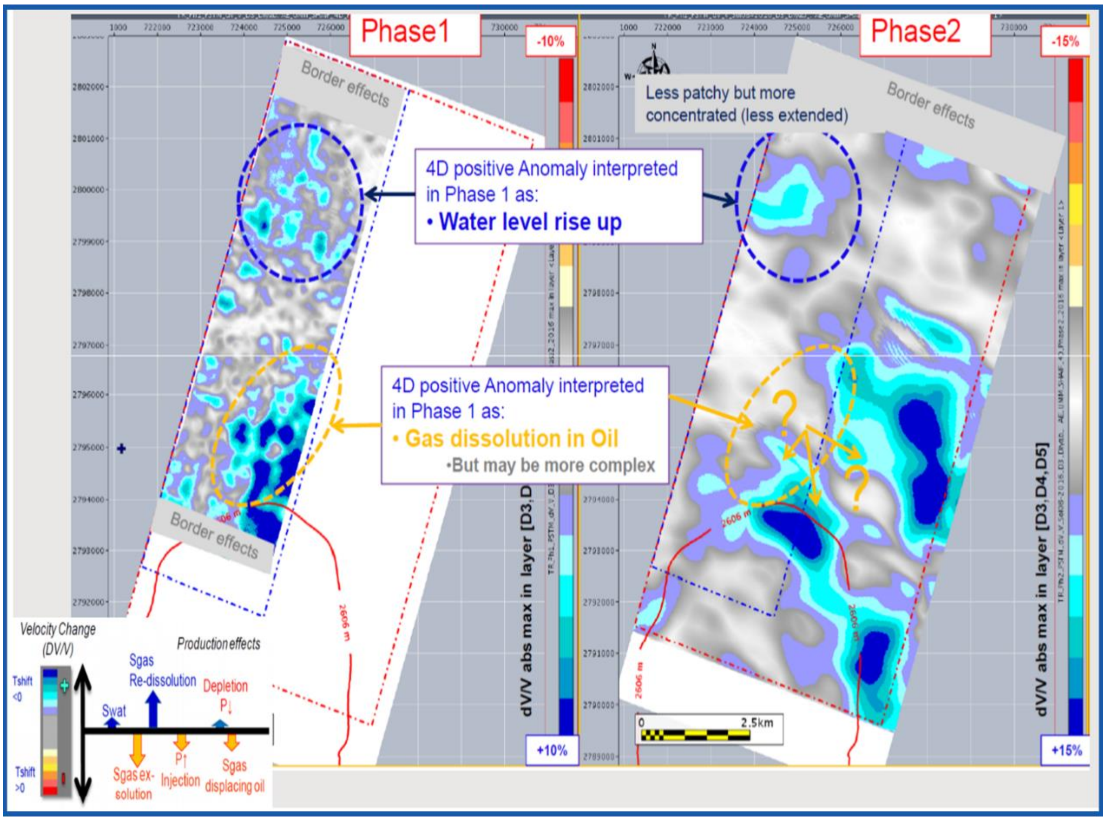


Figure 1.4 Case II; Phase 1 /Phase 2 comparison of the reservoir zonation (after Lafram et al., 2016).

## 1.5 Novelty of the Research

There are still two perceptions in the industry that 4D seismic in carbonate has very limited success. The first is the heterogeneity of carbonate, which is a high velocity deposit and has very subtle changes in velocity and density. These are the two essential properties required to detect 4D seismic signatures. The second is the repeatability of the seismic acquisition, which must be perfectly accurate to obtain meaningful 4D seismic in general and in carbonate rocks in particular. However, the novelty of this research has proven that there is something other than these perceptions.

The 4D feasibility of this research has shown that 4D signal capture is higher than 4% (the industry standard capture threshold). Second, the development of best practices for 4D seismic studies in general, and the creation of optimal 4D seismic co-processing in the case of low seismic acquisition repeatability in carbonate reservoirs in particular. Optimal 4D seismic co-processing, which is the main objective of this research, could improve the repeatability of seismic acquisition, which is extremely difficult to ensure in the offshore fields of Abu Dhabi (UAE).

The full integration of the three cases of this research, 4D feasibility, joint processing, inversion and matching with reservoir performance in seismic time-lapse is an unprecedented novelty in the industry and an outstanding outcome of this research.

### 1.6 Layout of Thesis

The background of the research and the research objectives are explained in Chapter 1. Chapter 2 covers the previously published work on 4D seismic co-processing, pre-stack depth migration (KPSDM versus LSM), followed by the theoretical aspects of least-square migration algorithm. In Chapter 2 as well, the 4D seismicity in carbonates and the characteristics of the seismic 4D metrics attributes and their corresponding theoretical background are highlighted. Chapter 3 describes the seismic and borehole data and related documents that form the input for this research, as well as the research methodology of this study. Chapter 4 (Results and Discussion) presents the outcomes of the petroelastic model and the 4D feasibility study. The pilot seismic volumes analysis of case II is illustrated and highlights the seismic 4D co-processing workflows of this research of the three different offshore cases in Abu Dhabi, UAE.

Chapter 4 then also presents the geometric and metric attributes of 4D seismic for the processing results of the three cases. The results of dynamic 4D warping of the seismic traces and seismic inversion are also explained in Chapter 4. The application of machine learning to support the processing and inversion results is also accentuated in Chapter 4. Finally, the unprecedented research processes are highlighted by matching the outstanding results with reservoir performance, fluid exchange, and pressure changes over time of the 4D seismic surveys. Chapter 5 presents the conclusions of the research, the contribution of the research to the industry, and the recommendations for future seismic 4D investigations in carbonate reservoirs.

# CHAPTER 2

# LITERATURE REVIEW

## 2.1 Introduction

The literatures contain many previously published papers on time-lapse seismic monitoring, most of them on clastic reservoirs and only a few on heterogeneous carbonate reservoirs. For the different approaches used in this research, the literatures covering these approaches are highlighted by presenting different algorithms for 4D seismic data processing and pre-stack depth migration with their respective mathematical backgrounds. A review of publications on 4D seismic in carbonate reservoirs and the diagnostic 4D seismic metric attributes that should be investigated as a verifier to improve seismic acquisition repeatability during 4D seismic co-processing, especially when seismic acquisition repeatability is low. Very recent publications from 2022 were also discussed, highlighting the new seismic industry trend of the 4D seismic carbonate for the future.

## 2.2 4D Seismic Data Processing

The processing of 4D seismic data is challenging when the acquired data set contains inherent variability that obscures the expected time-lapse signal (Fischer et al. 2013). Accurate processing of seismic 4D time-lapse data, either pre-stack or post-stack, with a minimum number of matching filters can greatly improve the 4D seismic data interpretability. Seismic 4D processing pathways can be broadly divided into three main categories (Lumley et al. 2003), as shown in Table 2.1:

Table 2.1 4D Seismic Processing Routes.

| **Post-Stack Cross Equalization** | **Pre-Stack Parallel Processing** | **Simultaneous 4D Pre-Stack Processing** |
|---|---|---|
| Input data are: 3D seismic migration volumes processed independently. | Input data are: Multi-vintage data sets either pre-stack processed or reprocessed. | The input data are: The multi-vintage data sets are merged or linked in many processing steps. |
| Need: Cross-equalization processing to improve seismic repeatability in the unmodified zone prior to 4D interpretation. | Need: Process them asynchronously with a similar or identical processing sequence. | Need: They are specially processed simultaneously to extract the processing operators that are derived and applied to the data of multiple vintages. |
| Data sets are not reprocessed pre-stack | Data sets are processed pre-stack | Data sets are processed pre-stack simultaneously |
| This type is commonly used to enhance legacy seismic data and clean up residual data from re-shoot or 4D design datasets. | This type is used to optimize the repeatability of the final product and for re-shoot and 4D design datasets. | This type of data collection is commonly used in 4D design projects. |

In 4D seismic processing, the non-repeatable noise must be suppressed before the 4D signal is revealed. There are many sources of non-repeatable noise, such as variable amplitude gains, frequency content, static shifts, waveform phase changes, and events that lie between different data vintages (Lumley et al., 2003). A series of matching filters are applied to the data sets to remove sources of such non-repeatable noise (Ross et al., 1996).

4D Seismic data acquisition and processing should ensure repeatability of seismic events with respect to non-reservoir intervals, while the only differential signal could be a phase change of the reservoir fluid. Therefore, data conditioning and compensation of the non-reservoir (overburden level) is extremely important and essential (Mitra et al., 2007). Mitra has also recommended that pre-stack conditioning and post-stack matching are extremely important for the true representation of 4D seismic data.

4D seismic joint processing are successive steps started with 4D seismic trace binning and the corresponding 4D pre-processing. Spatial repeatability is enhanced by 4D binning, while concurrent 4D pre-stack processing develops common operators of processing that use cross-equalization as an essential processing step. Time-lapse (TL) seismic interpretation is divided into two categories based on the characteristics of the interpreted data: Interpretation of data sets and seismic differences between vintages from all TL vintages (Nguyen et al., 2015).

## 2.3 Pre-Stack Depth Migration

In the presence of inhomogeneous subsurface illumination and irregular acquisition geometry, least-square pre-stack depth migration (LSM) can restore reflectivity with amplitude reliability and resolution likelihood better than the classical Kirchhoff or even RTM algorithm (Shao et al., 2017). LSM is a user-friendly technique for 4D seismic co-processing, but LSM alone cannot improve the repeatability of seismic acquisition. Seismic co-processing shall be started from the base and monitor raw seismic filed data.

A 4D seismic case study in West Africa over a sandstone reservoir in which the 4D seismic analysis was demonstrated from feasibility to reservoir characterization (Webb et al., 2019). However, the 4D co-processing method that fills the gap of poor repeatability of seismic acquisition has not been sufficiently elaborated. Pre-stack depth migration is a standard for seismic imaging, starting from the application of Kirchhoff migration in the early 1990s to the introduction of reverse-time migration (RTM) in the late 2000s (Huang et al., 2017). However, pre-stack depth migration algorithms might induce migration artifacts such as migration swings, narrow seismic bandwidth, and amplitude distortion (Gray, 1997).

This is even true for an advanced imaging algorithm such as RTM (Baysal et, al., 1983; Zhang and Zhang, 2009). Narrow seismic frequency range of depth migration often outcomes poor image illumination and resolution, because of the seismic imaging geometry and the processing technology limitations used (Liu et al., 2018). The applications of linear inversion in seismic imaging are widely known (Schuster, 1993; Nemeth et al., 1999; Prucha and Biondi, 2002). Least squares migration (LSM) aims to recover the true reflectivity of the Earth by determining the inverse of the forward modelling operator by minimising the square of the misfit between the observed data and the modelled data (Huang et al., 2017).

The LSM was proposed to overcome of the standard Kirchhoff migration limitations (Trantola, 1987; Schuster, 1993; Nemeth et el., 1999). The LSM method was applied to a 2D line CDP post-stack data in the Gulf of Mexico (courtesy of Mobile) and did show the improving of spatial resolution even when the data are not spatially under-sampled (Nemeth et el., 1999).

Moreover, least-square reverse time migration (LSRTM) is expected to enable relatively high-resolution imaging while maintaining amplitude by encompassing the inversion of the Hessian matrix. LSRTM was outstanding for use in the delineation of the reservoir and 4D seismic imaging compared to out-dated RTM and Fourier finite difference (FFD) migration (Xiao-Dong et al., 2017). Inhomogeneous subsurface illumination and irregular acquisition geometry might make standard Pre-stack depth migration (PSDM), e.g., Kirchhoff/RTM, unable to completely recover reflectivity with the likely amplitude fidelity and resolution, (Shao et al., 2017).

Shan Qu and Dirk Verschuur (2019) have proposed simultaneous joint migration inversion as an active tool combining a joint time-lapse data processing strategy for baseline and monitor surveys with the joint migration inversion method for reservoir monitoring. However, simultaneous joint inversion was not established to overcome the poor repeatability of data acquisition in terms of detectability of the 4D signals.

### 2.4 Theory of Seismic Imaging by Least-Squares Inversion

To understand the theoretical assumptions of least-square inversion, it is assumed that the observed data, $d_{obs}$ of seismic imaging are assumed to be exclusive of the Earth's reflectivity. The standard pre-stack depth migration produces an estimate of the reflectivity, $m$ as follows:

$$m = L^* d_{obs} \qquad (2.4.1)$$

Here the operator $L^*$ is the adjoint, the inverse of the forward modelling operator $L$. The standard depth migration produces the Earth structural image. However, this result often led to irregular illumination, low bandwidth, and low wavenumber content because migration is not the reverse modelling (Xiao-Dong et al., 2017). Unlike conventional migration (Equation 2.4.1), least square migration (LSM) resolves the modelling path inverse:

$$m = (L^* L)^{-1} L^* d_{obs} \qquad (2.4.2)$$

The above explanation in Equation 2.4.2 can be obtained using two separate methods; the first clearly calculates the matrix $L^*L$ and its equivalent inverse, while the second is alternatively an implied method that can be used iteratively to invert the operator $L$ and answering the minimization problematic through:

$$m = arg\,min\frac{1}{2}\|d_{obs} - Lm\|^2 \tag{2.4.3}$$

The iterative LSM algorithm description is summarized in Figure 2.1, which could be fulfilled in a migration/demigration context. Inversion iteration consists of a Born modelling (Cohen et al., 1986) and a migration. The LSM sequence starts with an original pre-stack depth migration, followed by a migrated image in Born's modelling, using the migrated image as the reflectivity model. If the difference between the modelled synthetic data and the observed data is big, the data remaining d_obs-d_syn is migrated and used to update the image m. In general, the inversion converges when the discrepancy is within a resilient threshold. The path of seismic LSM processing (Dong et al., 2017) is shown in Figure 2.1.

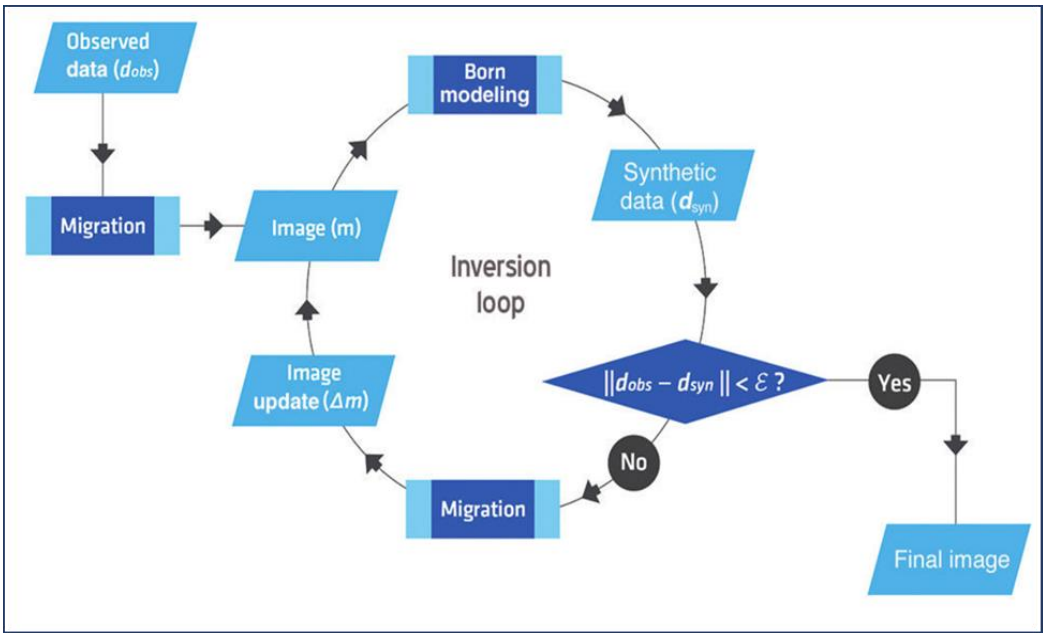


Figure 2.1 An iterative LSM algorithm workflow according to (Dong et al., 2017)

The Linear operator of original imaging Kirchhoff demigration:

$$d = Lr \tag{2.4.4}$$

Where $d$ is the acquired seismic data, $L$ is the acoustic operator of Kirchhoff's modelling, and $r$ is the subsurface reflectivity. Unravelling the inverse problem, $r = \mathrm{L}^{-1}\mathrm{d}$, produces the desired subsurface reflectivity. Nevertheless, the calculation of this traditional inverse is not possible in seismic acquisition reality. The usual alternate is to apply the adjoint $\mathrm{L}^{\mathrm{H}}$, of the forward operator $L$, to the acquired aseismic data (Claerbout, 1992):

$$m = L^H d \tag{2.4.5}$$

Where, $m$ is the original Kirchhoff migrated image.

This image will have a lot of migration artifacts and illumination problems since the inverse operator is not used. These shortcomings shall be overawed by minimization of a least squares cost function, $\mathrm{f(r)} = \|\mathrm{d} - \mathrm{lr}\|$. Nemeth et al., (1999) has developed a formulation that ties de-migrated modelled data with observed data to appraise the migrated image. Moreover, the solution of the least-squares normal equations provides the least-squares approximation to the subsurface reflectivity $\mathrm{r_{LS}}$:

$$r_{LS} = (L^H L)^{-1} L^H d \tag{2.4.6}$$

Here, $(L^H L)$ is called the Hessian operator and Equation 2.4.6 can be solved iteratively by using the conjugate gradient approaches. The Earth variable elastic properties could root absorption of seismic waves, resulting in phase distortion and amplitude attenuation. In straight acoustic migration, these $(Q)$ possessions are accounted for in both pre- and post-migration processing. However, the standard migration can be modified to directly compensate for these effects (Xie et al., 2009) by amplitude improvement and phase distortion elimination.

The least-squares Kirchhoff pre-stack depth migration process, visco-acoustic modelling that includes seismic absorption, the quality factor Q of the medium, could be cascaded on top of the LSM (Perrone et al., 2018). The inclusion of Q in the least squares migration takes a different approach to solving the amplitude data quality problem mentioned previously by altering the modelling in Equation 2.4.4:

$$d = L_Q r \tag{2.4.7}$$

Where, $L_Q$ signifies the Kirchhoff visco-acoustic modelling operator (Wu et al., 2017) and this could solve the normal equations to gain a new type of equation (Equation 2.4.6) that comprises $Q$-compensation:

$$r_{LS} = \left(L_Q^H L_Q\right)^{-1} L_Q^H d \tag{2.4.8}$$

The migration and de-migration runs associated with iteratively solving equations (2.4.6) or (2.4.8) are expensive from a computational perspective, which raises the question: What can be a reasonable, cost-effective method? Let us start by substituting Equation 2.4.5 into Equation 2.4.8 and provide:

$$r_{LS} = (L^H L)^{-1} m \tag{2.4.9}$$

With using this equation, the least squares approximation of reflectivity is an inverse Hessian, $(L^H L)^{-1}$ operator representing the filtered version of the migrated image. The application of the inverse Hessian matrix operator to the migration is to reduce the image artifacts due to the non-repeated source and receiver locations. Guitton (2004) proposed that could be done with non-stationary matching filters following a de-migration/re-migration process. The effect on the migrated image of the cascade a) → c) is precisely the Hessian operator (Guitton, 2004), which is inverse to estimate through matching filters in d), and final application to a) (Table 2.2).

Table 2.2 Math of LSM Seismic Processing Workflow after Perrone et al., 2018

| Processing Step | Equation |
|---|---|
| a) An initial migration, $m0$: | $m_0 = L^H d$ |
| b) A de-migration, $d0$, of the data in a): | $d_0 = Lm_0$ |
| c) A subsequent re-migration, $m1$, of the data in b): | $m_1 = (L^H d_0) = (L^H L)m_0$ |
| d) Design matching filters to match c) to a): | $m_0 = (L^H L)^{-1} m_1$ |
| e) Apply the matching filters from d) to the data in a): | $r_{LS} = (L^H L)^{-1} m_0$ |

The Curvelet domain Hessian operator was developed by both Khalil et al. (2016) and Wang et al. (2016 and is used to improve the stability and structural consistency of the LSM approach in the matching process.

Time-lapse (4D) technique has been developed in the last decade as an important tool for seismic imaging in hydrocarbon reservoir monitoring. Batzle and Wang (1992) outline the rock and fluid relationships importance; while Lumley (1995), Lumley and Rickett (2001), Calvert (2005), and Johnston (2005) have discussed the processing practical implementation. Lefeuvre et al., (2003),